NANO LETTERS

Letter

pubs.acs.org/NanoLett

Mechanisms of Local Stress Sensing in Multifunctional Polymer Films Using Fluorescent Tetrapod Nanocrystals

Shilpa N. Raja,[†,‡] Danylo Zherebetskyy,[†,△] Siva Wu,[†,§] Peter Ercius,[∥] Alexander Powers,[⊥] Andrew C. K. Olson,[†,⊥] Daniel X. Du,[#] Liwei Lin,[▽] Sanjay Govindjee,[○] Lin-Wang Wang,[†,◆] Ting Xu,[†,‡,⊥,◆] A. Paul Alivisatos,[*,†,‡,⊥,◆] and Robert O. Ritchie[*,†,‡,▽]

[†]Materials Sciences Division, Lawrence Berkeley National Laboratory, Berkeley, California 94720, United States

[‡]Department of Materials Science and Engineering, University of California, Berkeley, Berkeley, California 94720, United States

[§]Life Sciences Division and [∥]Molecular Foundry, Lawrence Berkeley National Laboratory, Berkeley, California 94720, United States

[⊥]Department of Chemistry, [#]Department of Chemical Engineering, [▽]Department of Civil and Environmental Engineering, and [○]Department of Mechanical Engineering, University of California, Berkeley, Berkeley, California 94720, United States

[◆]Kavli Energy NanoScience Institute, Berkeley, California 94720, United States

[△]Nanosys, Inc., 233 South Hillview Drive, Milpitas, California 95035, United States

S *Supporting Information*

ABSTRACT: Nanoscale stress-sensing can be used across fields ranging from detection of incipient cracks in structural mechanics to monitoring forces in biological tissues. We demonstrate how tetrapod quantum dots (tQDs) embedded in block copolymers act as sensors of tensile/compressive stress. Remarkably, tQDs can detect their own composite dispersion and mechanical properties with a switch in optomechanical response when tQDs are in direct contact. Using experimental characterizations, atomistic simulations and finite-element analyses, we show that under tensile stress, densely packed tQDs exhibit a photoluminescence peak shifted to higher energies ("blue-shift") due to volumetric compressive stress in their core; loosely packed tQDs exhibit a peak shifted to lower energies ("red-shift") from tensile stress in the core. The stress shifts result from the tQD's unique branched morphology in which the CdS arms act as antennas that amplify the stress in the CdSe core. Our nanocomposites exhibit excellent cyclability and scalability with no degraded properties of the host polymer. Colloidal tQDs allow sensing in many materials to potentially enable autoresponsive, smart structural nanocomposites that self-predict impending fracture.

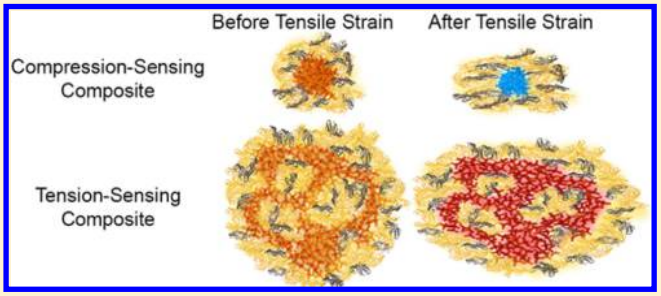

KEYWORDS: *Nanocomposite, tetrapod nanocrystal, polymer, sensor, mechanical, fluorescence spectroscopy*

As premature failure of structural components invariably results from the initiation and incipient growth of small cracks,[1−3] there is a vital need for autoresponsive structural materials that potentially self-detect and self-respond to environmentally induced mechanical damage.[4] Such materials have a built-in potential to prevent catastrophic failure in service applications.[5] However, current technologies that can provide for the early self-detection of local stresses associated with incipient cracks are extremely limited.[6,7] Mechanophoric dyes and piezoresistive materials, for example, are only effective at the millimeter length-scale with relatively low sensitivity;[8−11] furthermore, such techniques are very challenging to implement "in the field".[1,6−15] In addition, many conventional sensing techniques adversely affect the properties of the host material.[1,5−7,16] A visible-light, nanoscale sensor with the ability to be embedded into a variety of "smart" structural materials without causing such degradation would be particularly appealing for the potential sensing of impending fractures in service.[5] Furthermore, mechanical stresses exerted by biological tissues can be signatures of disease.[17] Thus, such a sensor, if embedded into soft polymers,[18,19] could also potentially be of significant use in biological applications such as sensing of stresses in cancer cell proliferation.[7,20]

Colloidal semiconductor quantum dots display a multitude of size and shape-dependent properties, enabling their use in a variety of electronic and optical applications.[21] The ability to tune their size and shape, and in particular the ability to create branched nanoheterostructures, provide further opportunities to take advantage of their special behaviors.[22] One such opportunity is the creation of functional nanocomposites with specific "smart" characteristics, such as shape-dependent

Received: May 10, 2016
Revised: July 5, 2016
Published: July 13, 2016

DOI: 10.1021/acs.nanolett.6b01907
Nano Lett. 2016, 16, 5060−5067

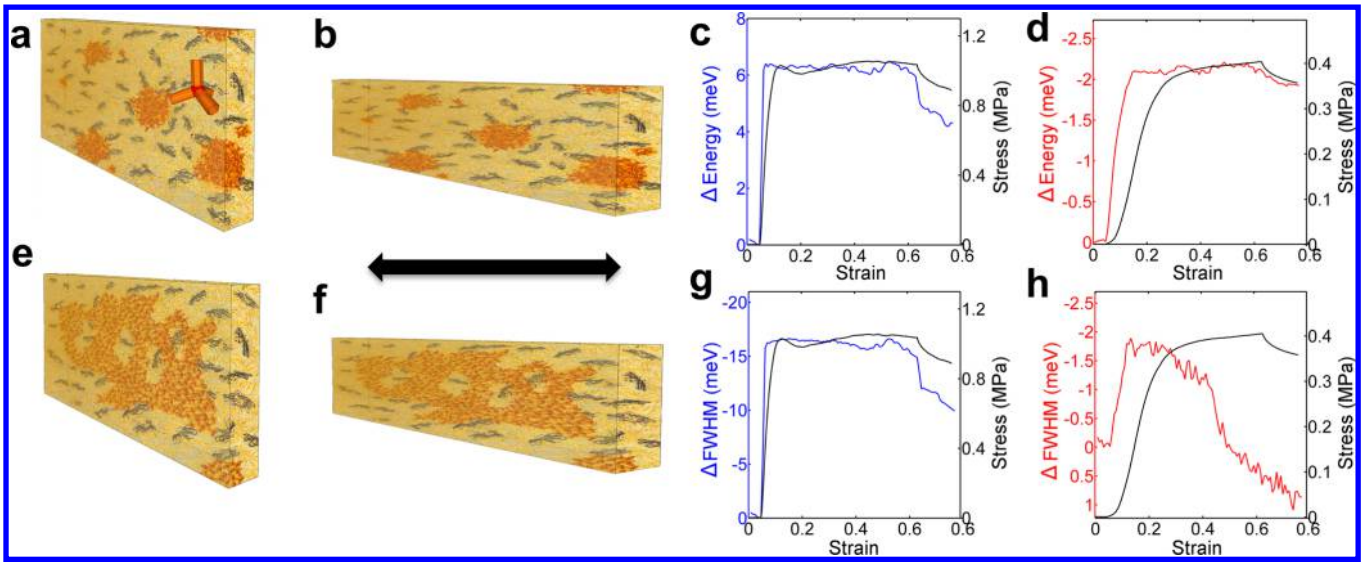

Figure 1. Schematic microstructures and simultaneous mechanical and fluorescence tensile stress−strain curves for compression- and tension-sensing tQD-SEBS polymer nanocomposite films. (a,b) Schematics of the microstructures of tQD-SEBS compression-sensing film (a) before and (b) after application of tensile stress. Yellow regions represent PE-B, black regions represent PS, and orange regions represent tQD clusters. Inset to (a) indicates schematic of single tQD nanocrystal. (c,d) Result of simultaneous fluorescence (blue line) and mechanical test (black line) for (c) emission maximum shift and (d) fwhm shift for compression-sensing film. (e,f) Schematics of the microstructures of tQD-SEBS tension-sensing film (e) before and (f) after application of tensile stress. (g,h) Result of simultaneous fluorescence (red line) and mechanical test (black line) for (g) emission maximum shift and (h) fwhm shift for tension-sensing film. Black double arrow indicates direction of applied tensile stress.

mechanical properties or self-healing properties upon exposure to radiation.[16,23,24]

The cadmium selenide−cadmium sulfide (CdSe-CdS) core/shell tetrapod quantum dot (tQD) is a particularly interesting system. Because of the tQD's bright photoluminescence and branched morphology in which the four long CdS arms confer a net stress on the CdSe core upon deformation, the tQD exhibits a unique photoluminescence stress response[25] as seen in previous studies in diamond anvil cells,[26] under atomic force microscope (AFM) tips[27] and in semicrystalline polymers.[5,7] Owing to its nanoscale size and unique shape,[26] the tQD can provide a far higher spatial resolution of stresses than most existing technologies.[7,28]

Prior studies on the tQD as a polymer stress sensor have been limited by low sensitivity and the detection of only tensile stresses and no self-reporting of local composite morphology.[5,7] Furthermore, sensing was also only demonstrated in polymer fibers, rather than films,[5,7] and was restricted by an inability to correlate optical and mechanical data as these measurements could not be performed simultaneously[5,7]

Here, we present the tQD as a detector of nanoscale compressive and tensile stress when embedded into widely used, low-cost smart structural block copolymer films. We perform optical sensing during mechanical testing in real time and show quantitatively the reasonable degree of matching between optical and mechanical curves. For the first time, we illustrate sensing in terms of both photoluminescence emission-maximum and full width half-maximum (fwhm). The tQD responds to stress via changes of its energy band gap,[26] with the response coming mostly from its CdSe core due to type I band alignment between the core and the CdS arms.[29] Tensile stress decreases the band gap by pulling apart the bonds in the tQD core, while uniform compression increases the band gap by moving the ions in the CdSe core closer together.[26] The photoluminescence emission spectra measured from tQDs embedded in the polymer matrix is then shifted to higher or lower frequency (blue- or red-shift, respectively) allowing for a direct measure of local stress. We show that tensile stress applied to densely packed tQDs in polymers results in a blue-shift of the tQD photoluminescence emission maximum due to uniform compression of tQD cores, while tensile stress applied to loosely packed tQDs in polymers results in a red-shift of the tQD photoluminescence emission maximum due to a net core tension. This phenomenon arises from the unique ability of tQDs to self-report subtle changes in nanoscale dispersion and related changes in macroscopic composite mechanical properties with a switch in optomechanical response from red-shifting to blue-shifting when tQDs are in direct contact. A polymer-embedded sensor that can self-report its own dispersion would be of broad utility for nanocomposite design and to the best of our knowledge has never been reported.[30,31] Because of the unique stress amplification effects of the tQD, the film sensors have 2 orders of magnitude higher stress response than bulk CdSe.[8,11,12,32,33] Using density functional theory, finite-element modeling, and experimental techniques such as transmission electron microscopy (TEM), electron tomography, characterization of fluorescence as a function of tensile stress, time-resolved photoluminescence spectroscopy, atomic force microscopy (AFM), and soft-X-ray scattering, we reveal the nanoscopic origins of the tQD photoluminescence shifts. Furthermore, we show that tQDs do not degrade the mechanical properties of the polymer films and have unchanged photoluminescence properties even after a year of storage in air; moreover, the film preparation method is scalable to industrial processing. The tQD sensor can be customized to sensing local tension or compression by changes in room-temperature processing. tQDs provide a highly sensitive material to potentially monitor stress distributions around cracks in structural nanocomposites for in service applications and can potentially be implemented in the field using low-cost, portable equipment. As previous work has shown the ability of spherical nanoparticles to diffuse to growing cracks in materials

DOI: 10.1021/acs.nanolett.6b01907
Nano Lett. 2016, 16, 5060−5067

and diminish their ability to propagate,[4] the findings of this work could possibly allow for diverse "smart", dispersion-reporting, self-healing structural tQD-spherical nanoparticle−polymer nanocomposites that can sense local and overall composite mechanics as well as potentially detecting and preventing their own fracture.[7,24]

The composites in this work were prepared by mixing tQDs in chloroform with the widely used structural block copolymer, poly(styrene-ethylene-butylene-styrene) (SEBS). The SEBS consisted of 60% polystyrene (PS) and 40% poly(ethylene-butylene) (P-EB) with an molecular weight of 117 000 Da.[34] All tQDs were incorporated with their native alkyl chain ligands (no ligand exchange was performed in this study) at a concentration of 20% by weight, or 5% by volume, into SEBS using a solvent-casting method under two separate processing conditions. One set of composites was dried under a vigorous nitrogen flow with the drying process completed within 1−2 min. We refer to these as tension-sensing films due to their decrease (red-shift) in photoluminescence wavelength with applied tensile stress, which as we show below is due to tensile stress in the tQD cores. The other set of composites were allowed to dry slowly in ambient with the process completed in 1−2 h. We refer to these as compression-sensing films due to their increase in photoluminescence wavelength with applied tensile stress, which as we show below is due to volumetric compressive stress in the tQD cores resulting from direct contact between tQDs. Figure 1 shows schematic illustrations of the compression-sensing and tension-sensing films prepared via the two above-mentioned protocols before and after application of tensile stress. Likely due to the imperfect interface between the tQDs and SEBS,[30] tQDs partially phase separate to decrease polymer-tQD interfacial tension,[35] forming small dense assemblies in the compression-sensing films and sparse, larger ones in the tension-sensing films. The slightly better tQD dispersion observed in tension-sensing films may be due to the vigorous nitrogen flow during drying, which acts as a mixing agent to better disperse tQDs during drying. In both cases, tQD assemblies are uniformly distributed throughout the polymer films.

The fluorescence properties of both films were studied under tensile deformation using an inverted fluorescence microscope (Figure 1). Understanding of the tQD stress response requires knowledge of agreement between optical and mechanical tests. Here we examine the concept of tQD mechano-optical sensing by coordinating mechanical and optical data acquired simultaneously. Our composites were deformed uniaxially to a maximum strain of 60% and held to evaluate stress-relaxation behavior.

The mechano-optical sensing behavior, depicted in Figure 1, shows a fluorescence shift of the tQD-SEBS composites in the compression-sensing and tension-sensing films as a function of applied strain, along with the corresponding mechanical loading curves (black lines) (Supplementary Figure 1). The results of peak position and fwhm for compression-sensing nanocomposites (Figure 1c,d) indicate excellent agreement between the mechanical loading curve and the optical sensing curve. Most of the emission maximum shift occurs in the elastic region in which a slope of 8.6 ± 0.9 meV/MPa is measured as well as a maximum optical shift of 4.5 ± 0.4 meV. The fluorescence curve additionally shows variation in the nonlinear region and matches the exponential behavior of the mechanical stress relaxation well.

We also see fairly good opto-mechanical agreement in the tension-sensing composites (Figure 1f) although not as good as in the compression-sensing composites (Figure 1d). The maximum fluorescence red-shift occurred mainly in the elastic region, which had a slope of −2.4 ± 0.3 meV/mPa and a maximum optical shift of 1.3 ± 0.14 meV.

We find that for compression-sensing films, the fwhm of the spectra follows the stress−strain curve of the composite (Figure 1g). Additionally, the fwhm sensitivity in stress and strain −39 ± 5 meV/MPa and −300 ± 30 meV/strain, respectively, is significantly higher than previously reported tQD emission maximum response sensitivity.[7,16] This additional sensing mode is not observed in any of the tension-sensing films (Figure 1h) or in any previous studies in tQD fiber composites.[7,16] Unlike in the compression-sensing films, and as in previous work, the photoluminescence FWHMs in tension-sensing films exhibit a slight increase (Figure 1h) but do not track the stress−strain curve.[7,16]

All sensitivities, or pressure coefficients, reported in units of shift/stress (meV/MPa) show significant improvements over the values reported for bulk CdSe.[32,33] This is perhaps due to the unique geometry of the tQDs in which the CdS arms act as antennas that amplify and transfer stress from the environment to the CdSe core. Indeed, this was also seen in our finite-element simulations, as discussed below. Our tQD films sense stress with an optical deformation response 3 orders of magnitude more sensitive than previous tQD sensors,[5] making them equal or better in sensitivity than several other key local stress-sensing technologies (Supplementary Note 1).

The films exhibited nearly identical optical and mechanical properties even after a year of storage in air (Supplementary Figure 2). The sensing is very repeatable; 20+ cycles of stretching to ∼60% strain performed on the same sample led to nearly identical sensor responses with a return to the same baseline fluorescence fwhm and emission maximum in-between tests. This likely indicates that the tQDs are experiencing fully elastic deformation during the stress-sensing in the polymer.[27] Compared to control samples, the ductility and toughness of the compression-sensing and tension-sensing films were unchanged.

We investigated the possibility that the blue-shift under tension could be due to better Forster resonance energy transfer (FRET) efficiencies in close-packed aggregates. However, this is unlikely as we found no difference in photoluminescence rise time or initial lifetime decays[36,37] between compression- and tension-sensing films (Supplementary Figure 3).

The different, opposite, photoluminescence shifts in tension-sensing and compression-sensing composites are rather striking because the films only differ in their drying time. To investigate whether the microscopic structural differences between these two films were responsible for their disparate sensing behavior, transmission electron microscopy was used to determine their microstructures. The images shown in Figure 2 show that the two films exhibit very different morphologies. Qualitatively, the compression-sensing tQD films contain densely packed aggregates that appear darker than the tension-sensing aggregates in the TEM images. The tension-sensing aggregates are less dense and have a large number of 10−500 nm diameter inter-tQD regions, as seen in Figure 2b,d. Because of the fast diffusion constant of the polymer chains in solution during drying (>10^{17} cm^2/sec[38]) and the rate of the drying processes employed, these regions are likely filled with polymer. This was

DOI: 10.1021/acs.nanolett.6b01907
Nano Lett. 2016, 16, 5060−5067

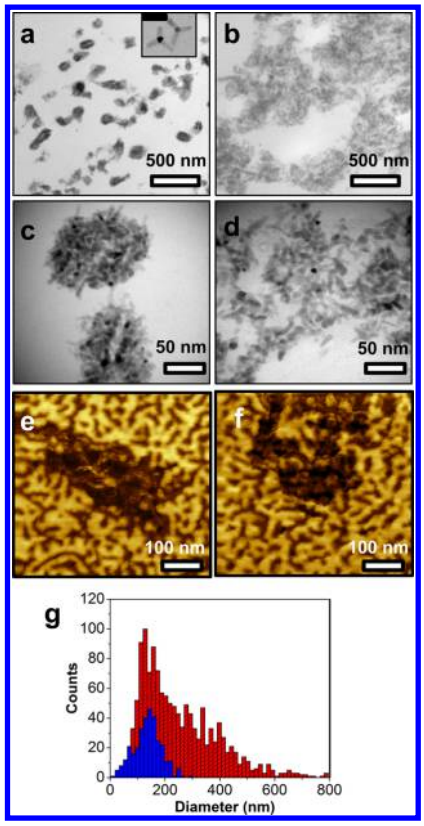

Figure 2. TEM and AFM of compression- and tension-sensing tQD-SEBS nanocomposites. (a,b) Low-magnification TEM micrographs of (a) compression-sensing and (b) tension-sensing films. Inset to (a) indicates tQDs before polymer encapsulation. Inset scale bar is 40 nm. (c) Higher-resolution TEM images of compression-sensing and (d) tension-sensing films showing that they are composed of tQDs. (e,f) AFM micrographs of (e) compression-sensing and (f) tension-sensing films. (g) Size distributions of diameters of tQD aggregates in compression-sensing and tension-sensing films. Blue and red histograms represent size distributions for compression-sensing and tension-sensing films, respectively.

confirmed by electron tomography (Figure 3), which shows that the inter-tQD regions are filled with matter consistent in contrast with the polymer material outside the aggregates. Figure 2g shows histograms of aggregate diameters for compression-sensing and tension-sensing aggregates, respectively, from several TEM images. In general, tension-sensing aggregates have a diameter approximately two times greater than compression-sensing aggregates. Figure 2g also shows that the quickly dried tension-sensing material contains some large aggregates as indicated by the asymmetric histogram with a large tail, while the slowly dried compression-sensing aggregates have a more symmetric size distribution. The change in packing density that results in a switch from red- to blue-shifting, or tension- to compression-sensing, is accompanied by a Young's modulus increase of a factor of 2. Thus, tQDs do not only report subtle changes in the nanoscale dispersion of the composite filler phase but also can serve as a visible-light indicator of associated changes in mechanical properties.

To investigate whether the polymer morphology and microdomain organization may have been altered by the different drying conditions, we acquired AFM phase images of the compression-sensing and tension-sensing aggregates. The AFM images are shown in Figure 2e,f with the same resolution and field of view. An entire compression-sensing aggregate is

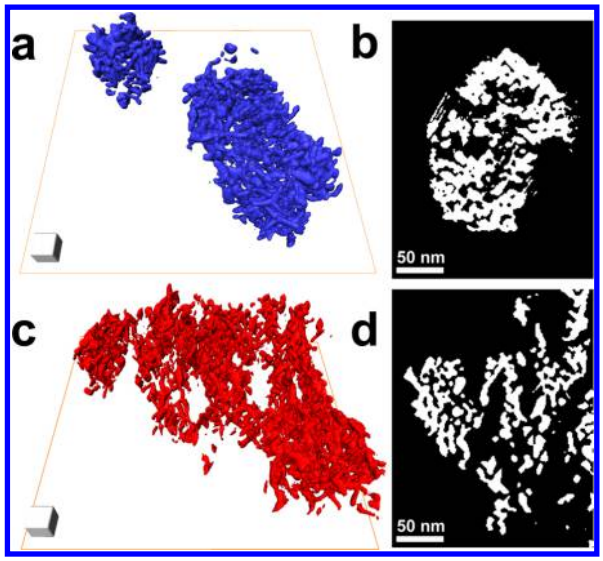

Figure 3. Electron tomography reconstructions of tQD-SEBS nanocomposites. (a,c) Perspective image of isosurface reconstruction of compression-sensing and tension-sensing aggregates, respectively, produced by electron tomography. White scale cube has 25 nm sides. (b,d) Thresholded 1.13 nm slices of the tomogram representative of the internal structure of the compression-sensing and tension-sensing aggregates, respectively.

imaged in Figure 2e but only part of a tension-sensing aggregate can be seen in Figure 2f. In the region around the aggregates, light represents polystyrene and dark represents P-EB, as described in more detail in the Methods section. The AFM results indicate a morphology with cylindrical and lamellar P-EB regions in a PS matrix and show little to no difference in the microdomain spacing and distribution of polymer around the aggregates in the tension-sensing and compression-sensing films, which was confirmed by ruthenium tetroxide staining.[39]

Traditional TEM projection images are sufficient to determine the large-scale (>100 nm) porosity inside the aggregates but the overlap of many tQDs in projection obscures their 3D distribution and the small-scale (<10 nm) inter-tQD regions. We utilized STEM electron tomography to determine the internal distribution of the tQDs and polymer inside of the aggregates. Figure 3a,c shows images of isosurface renderings of 3D electron tomography reconstructions for both the compression-sensing and tension-sensing composites (Supplementary Movies 1 and 2 show the 3D reconstructions). The tomography was performed using cryo-microtomed cross sections with a thickness (~70−90 nm) smaller than the diameter of the aggregates (~150 nm). The tomographic images revealed small regions of polymer ~10 nm in diameter that were inside the aggregates (Figure 3b,d) and not visible in the TEM projection images (Figure 2c,d). The analysis of small-scale porosity from each individual slice of the tomography reconstructions showed that the volume ratios of tQD/polymer (which we term tQD aggregate fill fraction, or packing density) in the aggregates were 50% ± 5% and 25% ± 2% for compression-sensing and tension-sensing aggregates, respectively. This small-scale porosity can be viewed as an approximation of the distance between adjacent tQDs, as tQDs have arm lengths of 26 ± 3 nm. These results illustrate that individual tQDs are about a factor of 2 farther apart in the tension-sensing aggregates than in compression-sensing

DOI: 10.1021/acs.nanolett.6b01907
Nano Lett. 2016, 16, 5060−5067

aggregates and that the tension-sensing aggregates have a factor of 2 times more polymer inside of them in terms of small-scale inter-tQD regions. They also indicate that in the aggregates the tQDs are in direct contact, separated only by their thin outer ligand coating[40−42] (Supplementary Figure 4a,b). Results on resonant soft X-ray scattering of the respective samples are given in Supplementary Note 2 and Supplementary Figure 4c. Only red-shifts were seen at a variety of tQD packing densities below 50%, including homopolymers (i.e., polymers formed from a single monomer) and cases in which tQDs are singly dispersed (Supplementary Figure 1). Because of the colloidal nature of tQDs and their ability to self-report whether they are in direct contact, they potentially could enable autoresponsive, multifunctional structural nanocomposites that would self-predict local and bulk mechanical properties as well as impending fracture.

Having shown how the aggregates differ structurally, we now use electronic structure calculations to illustrate the underlying mechanism of photoluminescence shifts due to an applied mechanical stress. We performed atomistic density functional theory (DFT) simulations on tQDs with zinc-blende CdSe cores of 2.8 nm, wurtzite CdS arms of 4.2 nm in length and 1.9 nm in diameter, containing 4245 atoms with the chemical formula $Cd_{272}Se_{297}/Cd_{1132}S_{1116}$, with pseudohydrogen passivation. Because the experimentally most relevant tQD size is too big (hundreds of thousands of atoms) for calculations at the DFT level (atomistic), we carried out calculations for a model of a smaller tQD. Electronic structure effects due to mechanical distortions should be qualitatively similar for nanoparticles of the same geometrical shapes made of the same material. This is described in more detail in Supplementary Note 3 and Supplementary Figure 5. We found that both the conduction band minimum state and valence band maximum state are located in the CdSe core, which is in agreement with experiments.[29] To simulate stressed tQDs, an atomistic valence force field model[43] was used to calculate the atomic positions under different stresses. The different stress states include uniform bond distance scaling (isotropic compression and tension) and uniaxial pushing or pulling at the tips of the four arms (uniaxial compression and tension) (Figure 4) (see Supplementary Note 3 for details on stress states, such as torsion).

Only the uniform, volumetric compression case results in a blue-shift. Among the red-shift cases, the situation most relevant to the experiment is uniaxial tension. The local strain of the tQD under uniaxial tension is shown in Figure 4d. Near the CdSe core, there are both positively and negatively dilated regions. This makes the red-shift relatively small. Considering that 2.5% strain was applied, which is likely much higher than the experimental tQD strains due to imperfect stress transfer to the tQD,[30] the theoretically obtained band gap changes were much higher than the experimentally observed shifts. Supplementary Table 1 shows the changes in the valence band maximum and conduction band minimum under the different tQD deformations. In summary, the theoretical results revealed that only deformations that caused a net decrease in volume of the CdSe core produced a blue-shift of the energy levels.

To investigate how tQD core compression may arise under overall uniaxial tension of the polymer nanocomposite, we conducted voxel-based micromechanical finite-element analysis simulations of tQDs in a polymer matrix using the Finite Element Analysis Program (FEAP).[44] The simulations used

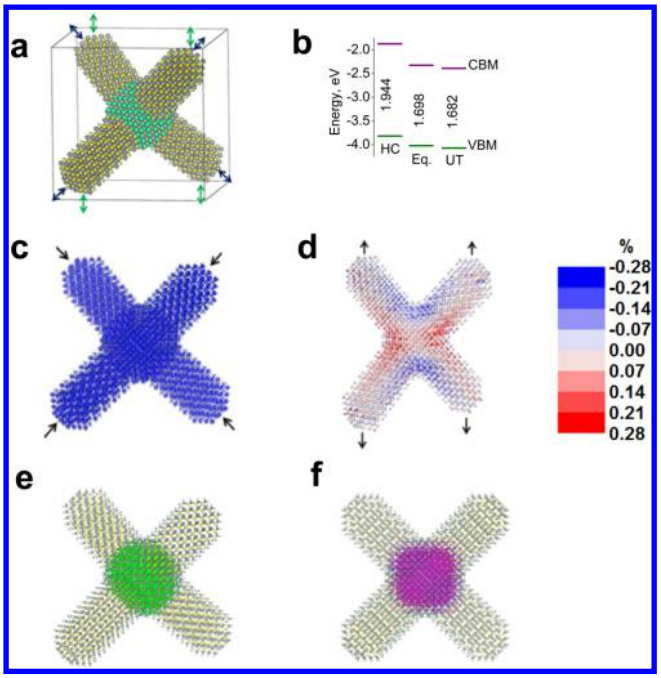

Figure 4. Valence force field simulations and density functional theory of energy levels of stressed tQDs. (a) Atomic structure of and schematic of stress application to modeled CdSe/CdS core-arm tQD/zinc-blende CdSe core. (b) Energy level changes of stressed tQDs. HC represents energy level changes for a tQD under hydrostatic compression, Eq represents the energy levels for a tQD at equilibrium (no stress), and UT represents the energy levels for a tQD under uniaxial tension. (c,d) Distribution of stresses in tQDs that are (c) compressed isotropically and (d) stretched uniaxially. Colorbar shows percent change in volume. (e,f) Equilibrium (unstressed) wave function charge densities of the valence band maximum and conduction band minimum, respectively.

periodic boundary conditions and net average uniaxial loads for a range of packing densities utilizing multiple random configurations to generate valid statistics. As the focus of the analysis was an elucidation of the mechanism leading to net compression of the core, two-dimensional simulations were performed to ease the cost and complexity. Previous comprehensive work considering comparing some nine 2D and 3D unit cells showed only a 5−10% difference in the results for elastic modulus; because the majority of the blue-shifts and red-shifts that are observed occur in the elastic region, this is further justification for use of a 2D finite element model.[45]

Two example configurations are illustrated for low (Figure 5a) and high (Figure 5b) tQD aggregate volume fractions, or packing densities. Figure 5c shows the typical pressure response of a CdSe core in the low packing regime; the integral of the pressure field is positive, indicating the overall response is tensile. In contrast, Figure 5d shows a typical pressure response in a CdSe core in the high packing regime; the integral of the pressure field is negative indicating the overall response is compressive. Though it varied significantly depending on the tQD location in the aggregate, the average core stress across all cores and configurations was of similar magnitude for net compressive and net tensile cases. The mechanism leading to the compressive case is one in which the CdS arms strongly interact due to close proximity and have a large span in the direction orthogonal to the loading, that is, tQDs serve as sensors of nanoscale dispersion with a dichotomy in response characteristic (e.g., red-shift or blue-shift, or compressive or

DOI: 10.1021/acs.nanolett.6b01907
Nano Lett. 2016, 16, 5060−5067

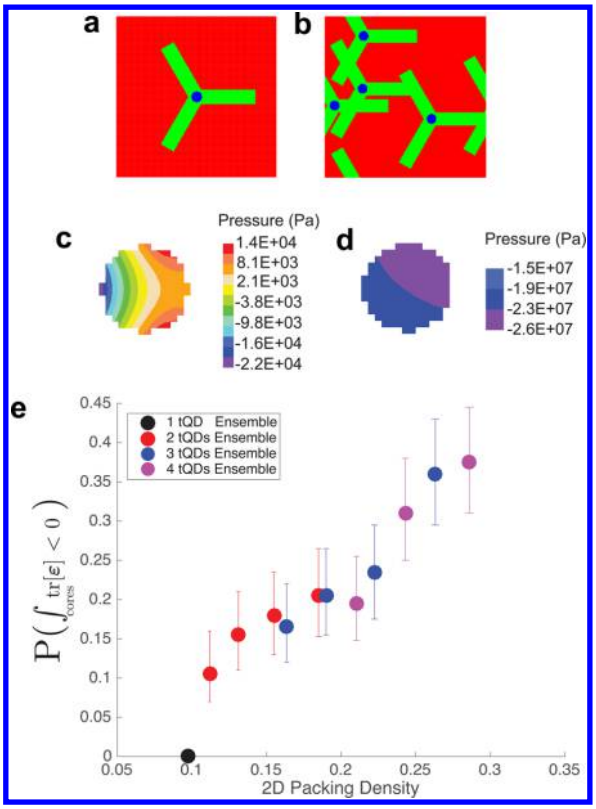

Figure 5. Finite element analysis of compression-sensing and tension-sensing tQD aggregates in a polymer under tension. (a,b) Finite element analysis images of low density (tension-sensing) and high density (compression-sensing) tQD aggregate unit cells. In the configurations shown, compression-sensing aggregates have 28% tQDs by area and an applied uniaxial stress of 0.53×10^4 Pa, while simulated tension-sensing aggregates have 9.6% tQDs by area and an applied uniaxial stress of 0.14×10^4 Pa. (c) Pressure map of a tension-sensing tQD core from (a). (d) Pressure map of a compression-sensing tQD core from (b). (e) Probability that a given tQD configuration at a given tQD volume fraction, or packing density, in an aggregate will result in a net average volumetric compression in the tQD cores. Black, red, blue, and magenta, respectively, represent ensembles with one, two, three, and four tQDs.

tensile) depending on whether or not adjacent tQDs are interacting.

By simulating a large ensemble of configurations (~200), we gain a statistical estimate of the probability that a given packing density will lead to a situation in which uniaxial tension gives rise to a net volumetric compression of the CdSe cores in an aggregate (see Supplementary Note 4 for details). As shown in Figure 5e, high packing densities lead in a near linear fashion to higher probabilities of net compressive cores over the range of packing densities from ~10 to ~30% (the upper limit of what can be sensibly simulated in two dimensions).

The finite-element analysis reveals a substantial core stress amplification of up to a few orders of magnitude in the tQD for both volumetric compression and tensile stress cases, qualitatively consistent with experimental observations.

In summary, we have presented here a tQD/polymer nanocomposite system produced by low-cost, scalable colloidal processing that can act as a local sensor of tensile or compressive stresses. The stress is measured as shifts in the emission maximum and the full width at half-maximum of the photoluminescence spectra and is readily measurable in structural parts in service using commonly available portable spectrometers and light sources (see Supplementary Note 5). We show the unique capacity of tQDs to respond to subtle changes in their own nanoscale dispersion and mechanical properties with a switch in optomechanical response when tQDs are in direct contact. The sensitivity of the responses to deformation is 3 orders of magnitude greater than for current state-of-the-art tQD sensors and approaches or exceeds existing technologies. Moreover, the inclusion of tQDs in the polymer does not degrade the mechanical properties of the polymer matrix, and there is no reduction in response over >20 cycles of deformation. Simulations show that blue-shifts and red-shifts are due to compression and tension of the tQD core, respectively, during tensile deformation of the entire nanocomposite. The solution-processed tQD merges colloidal synthesis, interfacial tunability, and high sensitivity due to its geometry-borne stress-amplification. The tQD enables facile, scalable introduction into composite materials combined with effective local and bulk sensing capabilities. The tQD's ability to self-detect its own nanoscale dispersion in a composite results in a unique optical nanosensor that can self-report local as well as macroscopic composite properties, a potentially important characteristic for the design of "smart" polymer nanocomposites. On the basis of the previously established ability of spherical nanoparticles to diffuse to cracks in polymers and diminish their ability to propagate,[4] the results in this work could also engender tQD-spherical nanoparticle nanocomposites that could serve as multifunctional, autoresponsive, self-healing, structural parts potentially capable of predicting their own failure in service.[4,24]

Methods. CdSe-CdS tQDs were prepared as before.[36] The tQDs had arm length of 26 ± 3 nm and diameter of 6 ± 0.8 nm. SEBS was provided by Kraton (MD 1537) and dispersed in chloroform (Sigma-Aldrich) to create solutions of 150 mg of SEBS/~10 mL of chloroform for compression-sensing films and 25 mg of SEBS/~2 mL of chloroform for tension-sensing films. tQDs coated with native hydrophobic ligands were dispersed in chloroform and added to the polymer solutions at concentrations of 20% by weight/5% by volume of polymer. These precursor solutions were cast into glass Petri dishes for compression-sensing films and allowed to dry under ambient conditions followed by placing under vacuum. The drying process took 5−8 h. For tension-sensing films, precursor solution was added to a glass vial and subjected to a highly vigorous flow of nitrogen gas resulting in film drying occurring within 1−2 min.

The ~75−100 μm thick films were cut into strips 3−20 mm long × 1−3 mm wide for tensile tests and were clamped using flat grips into a tensile rig employing a Mark-10 0.5 N load-cell. A screw-driven stage connected to a controller (OptoMike OMEC−2BF) was used at a strain rate of 5×10^{-03} s^{-1}. Nineteen trials were performed for compression-sensing films and 13 trials for tension-sensing films. Tests were performed by stretching the sample to a strain of ~0.6 and holding for 28.5 s for stress relaxation. To assess repeatability, the same film was cycled >20 times.

To monitor fluorescence while stretching, the rig had a hole for laser passage and was mounted onto a metal plate for stability. We used an inverted fluorescence microscope with a spectrometer (Acton, SpectraPro-3001) and CCD (Princeton, 7509-0001). Exposure times of 1 s were used to collect spectra with 0.6 s between frames. We used 488 nm Ar+ laser excitation (Lexel Laser, Inc., 95) with 1 W power and 150 μm

DOI: 10.1021/acs.nanolett.6b01907
Nano Lett. 2016, 16, 5060−5067

spot size. We excited/measured photoluminescence from the core due to the type I band alignment, which localizes the electron and hole to the core, and to our 488 nm excitation.[36] Spectra were collected over the laser spot and fit to single Gaussians. Change in emission was defined as the difference between the peak position at time t and at zero strain.

For TEM, sections ∼70−90 nm were cut from ∼100 um thick films using an RMC MT-X Ultramicrotome (Boeckler) at cryogenic temperature and picked up from water onto copper grids. Staining was performed using RuO_4 to darken PS regions.[31] Stained sections were imaged using a 200 kV Tecnai G220 S-TWIN. Unstained sections were imaged using a 200 kV Tecnai G2. AFM samples were prepared similarly and were not stained. AFM images were obtained with a scanning probe microscope "NEXT" (NT-MDT) in amplitude modulation mode with a Si probe (spring constant 3.5 N/m). Height and phase images were recorded at the low force level (A_{sp} = 10 nm, A_0 = 12 nm) and high force (A_{sp} = 10 nm, A_0 = 24 nm) level. A_{sp} is set-point amplitude, while A_0 is free oscillation of the probe prior to sample interaction. Contrast in the phase images at low force varies from ∼0° to 10° and in phase images recorded at high force varies from ∼0° to 80°. We performed quantitative mapping of elastic modulus in Hybrid mode (a nonresonant oscillation mode in which the sample is modulated at 1.5 kHz). This allowed assigning of light-colored phase blocks to PS and darker blocks to softer PEB.

Tomography was performed using an FEI Titan 80-300 TEM operated in high-angle annular dark field STEM mode at 200 kV with a 10-mrad convergence angle. A tilt-series was acquired with 1.5° steps from ±70°, reconstructed using the IMOD software package. To calculate tQD/polymer packing density the 3D density was filtered with a 3 × 3 × 3 3D median filter and thresholded to distinguish tQD from polymer. The polymer/tQD volume ratio was calculated using all voxels within a boundary defined by a convex hull calculation. For average aggregate size and size distribution, a custom image segmentation MATLAB algorithm was developed to outline aggregates. More than 200 aggregates were counted for histograms. The diameter was computed from a circle with the same area as the aggregate. Compression-sensing aggregates had a diameter of 134 ± 5 nm, while tension-sensing aggregates had a diameter of 292 ± 9 nm. For finding tQD/polymer packing density from TEM images, we estimated the aggregate volume fraction of the polymer from the 2D aggregate fill factor and divided the nanoparticle volume fill fraction by this quantity.

Time-resolved photoluminescence lifetime measurements on compression-sensing and tension-sensing films were performed with a Picoquant FluoTime 300 employing a PMA 175 detector. An LDH-P-C-405 diode laser (excitation wavelength 407.1 nm) was used with a repetition rate of 1 MHz.

Reported errors are standard error of the mean, except for nanoparticle sizes, which are mean and standard deviation.

■ ASSOCIATED CONTENT

Supporting Information

The Supporting Information is available free of charge on the ACS Publications website at DOI: 10.1021/acs.nanolett.6b01907.

Three-dimensional electron tomography reconstructions of compression-sensing and tension-sensing aggregates in tetrapod quantum dot (tQD)-SEBS polymer nanocomposites.(MPG)

Three-dimensional reconstruction of tetrapods in compression-sensing material rotated around one axis. (MPG)

Materials and additional details of theoretical (finite element analysis, density functional theory) methods, more density functional theory and finite element calculations, resonant soft X-ray scattering, time-resolved photoluminescence, and other information and analysis. (PDF)

■ AUTHOR INFORMATION

Corresponding Authors

*E-mail: paul.alivisatos@berkeley.edu.

*E-mail: roritchie@lbl.gov.

Present Addresses

(S.W.) Viral Forensics, LLC, Berkeley, CA 94710.

(A.C.K.O.) ZS Associates, San Mateo, CA 94402.

Author Contributions

S.N.R., D.Z., and S.W. are co-first authors.

Notes

The authors declare no competing financial interest.

■ ACKNOWLEDGMENTS

Work on tQD nanocrystal−polymer nanocomposite preparation and optical, mechanical, and structural characterization was supported by the Director, Office of Science, Office of Basic Energy Sciences, Division of Materials Science and Engineering, of the U.S. Department of Energy under contract DE-AC02-05CH11231, specifically on the Inorganic/Organic Nanocomposites NSET Program (S.N.R., D.Z., L.W.W., T.X., A.P.A., and R.O.R.). Work done at the Molecular Foundry was provided by the Director, Office of Science, Office of Basic Energy Sciences, Division of Materials Science and Engineering, of the U.S. Department of Energy under Contract No. DE-AC02-05CH11231 (P.E.). L.L. was supported by National Science Foundation NSF Grant ECCS-0901864 for mechanical characterization support. The authors thank Andrew J. Luong for schematic figures, and Christina M. Hyland, Handong Ling, Michael Chen, Kari Thorkelsson, Turner J. Anderson, Arunima Balan, Jacob Olshansky, Cheng Wang, Chenhui Zhu, Sergei Magonov, Wendy Gu, Lindsey Hanson, Giulio Zhou and Katherine Evans for experimental assistance. We used the computational resources of the Oak Ridge Leadership Computing Facility at the Oak Ridge National Laboratory, which is supported by the Office of Science of the DOE under Contract No. DE-AC05-00OR22725, with computational time allocated by the Innovative and Novel Computational Impact on Theory and Experiment project.

■ REFERENCES

(1) Hanbücken, M.; Müller, P.; Wehrspohn, R. B. *Mechanical Stress on the Nanoscale*; John Wiley & Sons, 2011.

(2) Jarvis, E. A.; Hayes, R. L.; Carter, E. A. *ChemPhysChem* **2001**, *2* (1), 55−59.

(3) Li, X.; Chang, W.-C.; Chao, Y. J.; Wang, R.; Chang, M. *Nano Lett.* **2004**, *4*, 613−617.

(4) Gupta, S.; Zhang, Q.; Emrick, T.; Balazs, A. C.; Russell, T. P. *Nat. Mater.* **2006**, *5* (3), 229−233.

(5) Raja, S. N.; Olson, A. C. K.; Thorkelsson, K.; Luong, A. J.; Hsueh, L.; Chang, G.; Gludovatz, B.; Lin, L.; Xu, T.; Ritchie, R. O.; Alivisatos, A. P. *Nano Lett.* **2013**, *13* (8), 3915−3922.

DOI: 10.1021/acs.nanolett.6b01907
Nano Lett. 2016, 16, 5060−5067

(6) Kolle, M.; Lethbridge, A.; Kreysing, M.; Baumberg, J. J.; Aizenberg, J.; Vukusic, P. *Adv. Mater.* **2013**, *25* (15), 2239−2245.
(7) Choi, C. L.; Koski, K. J.; Olson, A. C. K.; Alivisatos, A. P. *Proc. Natl. Acad. Sci. U. S. A.* **2010**, *107* (50), 21306−21310.
(8) Pan, L.; Chortos, A.; Yu, G.; Wang, Y.; Isaacson, S.; Allen, R.; Shi, Y.; Dauskardt, R.; Bao, Z. *Nat. Commun.* **2014**, *5*, 3002−3002.
(9) Stevenson, A.; Jones, A.; Raghavan, S. *Nano Lett.* **2011**, *11* (8), 3274−3278.
(10) Lee, C. K.; Davis, D. A.; White, S. R.; Moore, J. S.; Sottos, N. R.; Braun, P. V. *J. Am. Chem. Soc.* **2010**, *132* (45), 16107−16111.
(11) Han, X.; Liu, Y.; Yin, Y. *Nano Lett.* **2014**, *14* (5), 2466−2470.
(12) Jin, X.; Götz, M.; Wille, S.; Mishra, Y. K.; Adelung, R.; Zollfrank, C. *Adv. Mater.* **2013**, *25* (9), 1342−1347.
(13) Zhao, Q.; Wood, J. R.; Wagner, H. D. *Appl. Phys. Lett.* **2001**, *78* (12), 1748.
(14) O'Shea, S. J. *J. Vac. Sci. Technol., B: Microelectron. Process. Phenom.* **1996**, *14* (2), 1383.
(15) Fitzpatrick, M. E.; Lodini, A. *Analysis of Residual Stress by Diffraction using Neutron and Synchrotron Radiation*; CRC Press: Boca Raton, FL, 2003.
(16) Raja, S. N.; Olson, A. C. K.; Limaye, A.; Thorkelsson, K.; Luong, A.; Lin, L.; Ritchie, R. O.; Xu, T.; Alivisatos, A. P. *Proc. Natl. Acad. Sci. U. S. A.* **2015**, *112* (21), 6533−6538.
(17) Dagdeviren, C.; Shi, Y.; Joe, P.; Ghaffari, R.; Balooch, G.; Usgaonkar, K.; Gur, O.; Tran, P. L.; Crosby, J. R.; Meyer, M.; Su, Y.; Webb, R. C.; Tedesco, A. S.; Slepian, M. J.; Huang, Y.; Rogers, J. A. *Nat. Mater.* **2015**, *14* (7), 728−736.
(18) Mikos, A. G.; Sarakinos, G.; Leite, S. M.; Vacant, J. P.; Langer, R. *Biomaterials* **1993**, *14* (5), 323−330.
(19) Levental, I.; Georges, P. C.; Janmey, P. A. *Soft Matter* **2007**, *3* (3), 299−306.
(20) Suresh, S. *Acta Mater.* **2007**, *55* (12), 3989−4014.
(21) Talapin, D. V.; Lee, J.-S.; Kovalenko, M. V.; Shevchenko, E. V. *Chem. Rev.* **2010**, *110* (1), 389−458.
(22) Choi, C. L.; Alivisatos, A. P. *Annu. Rev. Phys. Chem.* **2010**, *61* (1), 369−389.
(23) Raja, S. N.; Luong, A. J.; Zhang, W.; Lin, L.; Ritchie, R. O.; Alivisatos, A. P. *Chem. Mater.* **2016**, *28* (8), 2540−2549.
(24) Wu, D. Y.; Meure, S.; Solomon, D. *Prog. Polym. Sci.* **2008**, *33* (5), 479−522.
(25) Schrier, J.; Lee, B.; Wang, L.-W. *J. Nanosci. Nanotechnol.* **2008**, *8* (4), 1994−1998.
(26) Choi, C. L.; Koski, K. J.; Sivasankar, S.; Alivisatos, A. P. *Nano Lett.* **2009**, *9* (10), 3544−3549.
(27) Fang, L.; Park, J. Y.; Cui, Y.; Alivisatos, P.; Shcrier, J.; Lee, B.; Wang, L.-W.; Salmeron, M. *J. Chem. Phys.* **2007**, *127* (18), 184704.
(28) Jin, X.; Deng, M.; Kaps, S.; Zhu, X.; Hölken, I.; Mess, K.; Adelung, R.; Mishra, Y. K. *PLoS One* **2014**, *9* (9), e106991.
(29) Choi, C. L.; Li, H.; Olson, A. C. K.; Jain, P. K.; Sivasankar, S.; Alivisatos, A. P. *Nano Lett.* **2011**, *11* (6), 2358−2362.
(30) Bockstaller, M. R.; Mickiewicz, R. A.; Thomas, E. L. *Adv. Mater.* **2005**, *17* (11), 1331−1349.
(31) Balazs, A. C.; Emrick, T.; Russell, T. P. *Science* **2006**, *314* (5802), 1107−1110.
(32) Shan, W.; Walukiewicz, W.; Ager, J. W.; Yu, K. M.; Wu, J.; Haller, E. E. *Appl. Phys. Lett.* **2004**, *84* (1), 67.
(33) Li, J.; Wang, L.-W. *Appl. Phys. Lett.* **2004**, *85* (14), 2929.
(34) Raja, S. N.; Basu, S.; Limaye, A. M.; Anderson, T. J.; Hyland, C. M.; Lin, L.; Alivisatos, A. P.; Ritchie, R. O. *Materials Today Communications* **2015**, *2*, e33−e37.
(35) Sarkar, B.; Alexandridis, P. *Prog. Polym. Sci.* **2015**, *40*, 33−62.
(36) Crooker, S. A.; Hollingsworth, J. A.; Tretiak, S.; Klimov, V. I. *Phys. Rev. Lett.* **2002**, *89* (18), 186802−186802.
(37) Lunz, M.; Bradley, A. L.; Chen, W.-Y.; Gerard, V. A.; Byrne, S. J.; Gun'ko, Y. K.; Lesnyak, V.; Gaponik, N. *Phys. Rev. B: Condens. Matter Mater. Phys.* **2010**, *81* (20), 205316.
(38) Hiemenz, P. C.; Lodge, T. P. *Polymer Chemistry*, 2nd ed.; CRC Press: Boca Raton, FL, 2007.
(39) Ohlsson, B.; Törnell, B. *J. Appl. Polym. Sci.* **1990**, *41* (56), 1189−1196.
(40) Kim, J. Y.; Raja, S.; Stellacci, F. *Small* **2011**, *7* (17), 2526−2532.
(41) Tam, E.; Podsiadlo, P.; Shevchenko, E.; Ogletree, D. F.; Delplancke-Ogletree, M.-P.; Ashby, P. D. *Nano Lett.* **2010**, *10* (7), 2363−2367.
(42) Ye, X.; Zhu, C.; Ercius, P.; Raja, S. N.; He, B.; Jones, M. R.; Hauwiller, M. R.; Liu, Y.; Xu, T.; Alivisatos, A. P. *Nat. Commun.* **2015**, *6*, 10052.
(43) Pryor, C.; Kim, J.; Wang, L. W.; Williamson, A. J.; Zunger, A. *J. Appl. Phys.* **1998**, *83* (5), 2548.
(44) Taylor, R. L. *FEAP—A Finite Element Analysis Program*, version 7.5 User Manual; University of California at Berkeley: Berkeley, CA, 2005.
(45) Böhm, H. J.; Han, W. *Modell. Simul. Mater. Sci. Eng.* **2001**, *9* (2), 47−65.

DOI: 10.1021/acs.nanolett.6b01907
Nano Lett. 2016, 16, 5060−5067